

GUARANTEED CONFORMANCE OF NEUROSymbOLIC DYNAMICS MODELS TO NATURAL CONSTRAINTS

Anonymous authors

Paper under double-blind review

ABSTRACT

In safety-critical robotics and medical applications, it is common to use deep neural networks to capture the evolution of dynamical systems. This is particularly useful in modeling medical systems where data can be leveraged to individualize treatment. It is important that the data-driven model is conformant to established knowledge from the natural sciences. Such knowledge is often available or can often be distilled into a (possibly black-box) model M . For instance, the unicycle model (which encodes Newton’s laws) for an F1 racing car. Here, we wish to best approximate the system model while being only a bounded distance away from M with guarantees. We generate an unlabelled dataset to enforce conformance, where data is absent. Our first step is to distill all our data into few representative samples called memories, using the idea of a growing neural gas. Next, using these memories, we partition the state space into disjoint subsets and compute bounds for each subset utilizing M . This serves as a symbolic wrapper for guaranteed conformance. We argue theoretically that this only leads to bounded increase in approximation error; which can be controlled by increasing the number of memories. We experimentally show that on three case studies (Car Model, Drones, and Artificial Pancreas), our constrained neurosymbolic models conform to specified M models (each encoding various constraints) with order-of-magnitude improvements compared to the augmented Lagrangian and vanilla training methods.¹

1 INTRODUCTION

Deep neural networks (DNNs) are a complex class of function approximators which can succinctly capture the relationship between the current state-action pair and the next state. This is important in applications like Model-Based RL (MBRL) which is known to be more sample-efficient than model-free RL in standard control tasks (Moerland et al., 2020). In practice this is effective in various applications, like robotics and personalized medicine (Djeumou et al., 2022; Kushner et al., 2020; Shi et al., 2019), enabling system designers to comfortably achieve small approximation errors. A caveat comes with this flexibility—lack of generalization when pushed outside of the training distribution (Narasimhamurthy et al., 2019). A well-known example is non-conformance to Newton’s first law. The neural network dynamics model of a car should predict that, given zero throttle and when at rest, the car should continue to remain at rest. The model trained on real trajectory data in Goldfain et al. (2019) failed to conform to this property. A very similar property exists in the case of the glucose-insulin dynamics model for an artificial pancreas, a device for patients with type-1 diabetes. A well-accepted physiological property of the insulin-glucose dynamics was shown to be easily violated in Kushner et al. (2020). Such a DNN model could easily produce predictions that can be fatal for the patient. However, these challenges are much less prevalent in models which are typically informed by different scientific disciplines. Examples of this include models based on mechanical properties of robotic systems (Rajamani, 2011), aerodynamic properties of drag and lift (Mahony et al., 2012), physiological models of the human body (Man et al., 2014; Chen et al., 2015) and alike. Our goal is to use such models to inviscate a deep neural network into guaranteed conformance.

Related Work The problem of penalizing against constraint violation is well known and has received sufficient attention in the literature (Finzi et al., 2020; Márquez-Neila et al., 2017; Ravi et al., 2019). But, it broadly follows the path of including a penalty in the loss term when training a model. A more detailed summary and related literature are included in Appendix A. The benefit of our approach is

¹ Our code can be found at: https://github.com/neurosymbolic-models/constrained_dynamics

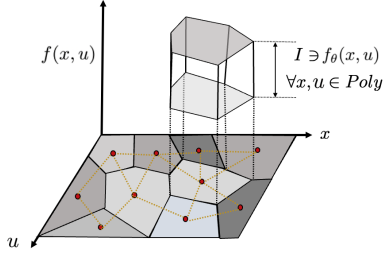


Figure 1: Depiction of our neurosymbolic algorithm. First, the input $\mathcal{X} - \mathcal{U}$ plane is partitioned into polyhedrons using a Neural-Gas. For inputs from each polyhedron, we generate sound under-approximations of the model M 's output. Next, we learn the dynamics f_θ that is constrained (by construction) to respect these interval constraints.

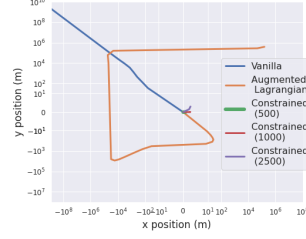


Figure 2: Trajectories generated from car dynamics models, starting at rest at the origin, with zero control inputs for 20 timesteps. Our neurosymbolic *constrained* models (with varying memories) respect Newton's first law of motion (and remain at rest) unlike *vanilla* and *augmented Lagrangian* neural networks that drift away from the origin.

that it is a numerical technique. It can soundly restrict the model's behavior and can work in tandem with any augmented Lagrangian technique well-known in the literature.

Our contributions can be listed as: 1) A novel memory-based method to constrain neural network dynamics models. 2) A theoretical guarantee that our memory-based constraining method guarantees conformance with only a bounded increase in approximation error. 3) Results on three case studies that show our method outperforms the augmented Lagrangian for constraint satisfaction by a few orders of magnitude.

2 PROBLEM FORMULATION

Consider a deterministic discrete time dynamical system given by: $x_{t+1} = f(s_t)$, where $\mathcal{S} := \mathcal{X} \times \mathcal{U}$, and $x \in \mathcal{X}$ is the state of the system, and $a \in \mathcal{A}$ is the action. Thus, $f : \mathcal{S} \mapsto \mathcal{X}$ is the possibly *unknown* map which captures state evolution. We assume access to a dataset $D = (s_0, x_1), (s_1, x_2), \dots, (s_{N-1}, x_N)$ drawn from distribution \mathcal{D} , and are related by the function f as shown above. In addition to estimating f with a function f_θ , it is desirable that the estimated model f_θ satisfies some natural constraints (Cranmer et al., 2020) expressed as a model constraint. The parameter $\theta \in \mathbb{R}^p$ is potentially the parameters of a neural network.

Definition 1 (Model Constraint). Assume knowledge of a model $M : \mathcal{S} \mapsto \mathcal{X}$, and a parameter $\delta \in \mathbb{R}$. The constraint $\psi_{M, f_\theta}^\delta : \mathcal{S} \mapsto \mathbb{R}$ is True iff $\psi_{M, f_\theta}^\delta(s) > 0$. Where, $\psi_{M, f_\theta}^\delta(s) := \delta - \|M(s) - f_\theta(s)\|_\infty$.

Here we assume M to be Lipschitz continuous with constant L ; but M may not be available in an analytical form. We state our problem next.

Problem Statement 1 (Constrained Neural Network). Find a function $f_\theta(\cdot) : \mathcal{S} \mapsto \mathcal{X}$, which minimizes the approximation error on dataset D , while satisfying the constraints given by $\psi_{M, f_\theta}^\delta$.

That is find $\theta^* = \arg\min_{\theta} \frac{1}{N} \sum_{i=1}^N \|f_\theta(s_i) - x_i\|_2$, subject to, $\psi_{M, f_\theta}^\delta(s) > 0$.

3 CONSTRAINING NEUROSymbOLIC DYNAMICS MODELS

Approach. The first step is to partition the input space into small enough input regions, and for each sub-region we estimate an interval under-approximation for the values of M which can satisfy $\psi_{M, f_\theta}^\delta$. Next, we train our function approximator f_θ to respect these interval constraints in each such sub-region. This is accomplished using a *constraining operator* Γ on f_θ . In the remainder of this section we outline the method for computing these sound under-approximations of M for each sub-region. The constraining operator Γ uses these bounds to build a symbolic wrapper. We show that the approximation error incurred due to this operator is bounded, in Appendix D. For most practical dynamical systems, we assume that the spaces \mathcal{S} and \mathcal{X} are embedded in the Euclidean spaces \mathbb{R}^t , and \mathbb{R}^d respectively, where $t \geq d$, and $t - d$ is the dimension of the action space.

Approximating Model Constraints. We use a *Neural Gas* to create prototypical samples which we refer to as *memories* in order to partition our state space. This identifies points in the input space \mathcal{S} , which induces a Voronoi tessellation. That is, a splitting of the space \mathcal{S} into a set of disjoint partitions $\mathcal{P}_\mathcal{S} = \mathcal{S}^1, \mathcal{S}^2, \dots, \mathcal{S}^k$. More details on this can be found in Appendix B. Our guarantees

Algorithm 1 Training a Constrained Neurosymbolic Dynamics Model**Input:** Dataset $\mathcal{D} = \{(s, x)_i\}_{i \in [N_{\mathcal{D}}]}$, model M , DNN architecture $f_{\theta}(\cdot)$ **Output:** Constrained neurosymbolic dynamics model $\Gamma(f_{\theta})(\cdot)$ **Parameters:** Number of memories n_{memories}

- 1: Generate input samples $\Omega = \{(s')_i\}_{i \in [N_{\Omega}]}$ // Generating unlabelled dataset for conformance.
- 2: $D|_{\text{inputs}} = \{(s)_i\}_{i \in [N_{\mathcal{D}}]} \cup \{(s')_i\}_{i \in [N_{\Omega}]}$ // combine inputs in both datasets
- 3: Memories \mathcal{A} , edges $\mathcal{E} \leftarrow \text{NeuralGas}(D|_{\text{inputs}}, n_{\text{memories}})$ // topology of input space
- 4: $\mathcal{S}^1, \dots, \mathcal{S}^j, \dots \leftarrow \text{VoronoiCells}(\mathcal{A}, \mathcal{E})$ // partitions in input space
- 5: Compute lower and upper bounds $I_{\text{low}}^j, I_{\text{up}}^j$ for each partition \mathcal{S}^j using M . These are the limits $\text{Lo}(s), \text{Up}(s)$ for each sample s belonging to a partition \mathcal{S}^j .
- 6: Train model $\Gamma(f_{\theta})(\cdot)$ in Equation (1) with wrapper limits above and self-supervised loss in Equation (2).

of constraint satisfaction is over the union of these subsets. For a Lipschitz continuous function M , acting on a subset \mathcal{S}_a it is possible to under-approximate its true output range on \mathcal{S}_a by a higher-order interval $[I_l, I_u]$. Given a Lipschitz constant, it is possible to bound the true error involved in this under-approximation by using the size of the set \mathcal{S}_a . This can be controlled by tuning the number of memories. We refer the reader to Appendix C for a detailed discussion on this. To summarize, we can obtain a constraint map as $\mathcal{C}_{M,\delta} : \mathcal{P}_{\mathcal{S}} \mapsto \mathcal{I}^d$, where \mathcal{I}^d is a d -dimensional interval in \mathbb{R}^d . For a subset in $\mathcal{P}_{\mathcal{S}}$, $\mathcal{C}_{M,\delta}$ returns an appropriate output range.

Function Approximation Error. Next, we define the constraining operator on a function using the above intervals. Assume an interval $I \subset \mathbb{R}^d$, and value $x \in \mathbb{R}^d$, then we define a projection in the following fashion along each dimension i , $\text{Proj}_I^i(x) := I_l^i$ when $x^i \leq I_l^i$; I_u^i when $x^i \geq I_u^i$; and x^i otherwise.

Definition 2 (Constraining Operator). A constraining operator $\Gamma_{\mathcal{P}_{\mathcal{S}}} : \mathcal{X}^{\mathcal{S}} \rightarrow \mathcal{X}^{\mathcal{S}}$ parameterized by the partition set - $\mathcal{P}_{\mathcal{S}}$, modifies functions to respect the corresponding interval constraints. For a function $F : \mathcal{S} \mapsto \mathcal{X}$, it can be defined in the following fashion :

$$\Gamma_{\mathcal{P}_{\mathcal{S}}}(F(s)) := \text{Proj}_{\mathcal{C}_{M,\delta}(\mathcal{S}_q)}(F(s)) \text{ where, } s \in \mathcal{S}_q \text{ and, } \mathcal{S}_q \in \mathcal{P}_{\mathcal{S}}$$

Hence, the constraining operator $\Gamma_{\mathcal{P}_{\mathcal{S}}}$ ensures that our estimated model f_{θ} which attempts to approximate the true function f , also respects the constraint $\psi_{M,f_{\theta}}^{\delta}$. Even though we assume that $f \models \psi_{f_{\theta},M}^{\delta}$, our approximation error in building the map $\mathcal{C}_{M,\delta}$ can affect the model approximation error $|f - f_{\theta}|$. This however as we show only leads to a bounded cost in approximation error. Which can be reduced by adopting finer partitions in $\mathcal{P}_{\mathcal{S}}$, that is increasing the nodes \mathcal{A} in the neural gas \mathcal{G} .

Theorem 1 (Approximation Error). Assume real and continuous functions $f, f_{\theta} : \mathcal{S} \rightarrow \mathcal{X}$, $\forall s \in \mathcal{S}$, if $\|f_{\theta}(s) - f(s)\|_{\infty} < \epsilon$, then $\|\Gamma_{\mathcal{P}_{\mathcal{S}}}(f_{\theta})(s) - f(s)\|_{\infty} < 2\epsilon + \alpha \max_{\mathcal{S}^k \in \mathcal{P}_{\mathcal{S}}} |\mathcal{S}^k|$, where α is some constant.

Proof. The proof can be found in Appendix D.

Training a Constrained Neurosymbolic Dynamics Model. We detail our constraining operator used in practice and our overall algorithm below. The inputs to the algorithm are a state transitions dataset D containing ((state, control), (next state)) pairs (s, x) , model M , and architecture $f_{\theta} : \mathcal{S} \rightarrow \mathcal{X}$.

Algorithm 1. First (line 1), we generate the unlabelled Ω dataset which consists of only inputs to the model $s' \in \mathcal{S}$ by sampling throughout the input space but with particular emphasis on relevant regions in \mathcal{S} . Next (lines 2, 3), we use the unsupervised neural gas algorithm (Martinetz et al., 1993; Fritzke, 1994) to obtain the memories. We partition the input space into voronoi cells around each memory (line 4). With model M , we obtain the upper and lower limits along each dimension of the output space (line 5). Finally, we can train the constrained neural network given below,

$$\Gamma(f_{\theta})(s) = \text{Lo}(s) + \sigma(f_{\theta}(s)) (\text{Up}(s) - \text{Lo}(s)) \quad (1)$$

where $\sigma(\cdot)$ is sigmoid. Our loss function is the augmented Lagrangian (Lu et al., 2021b) with label and constraint supervision on \mathcal{D} but only constraint supervision on Ω (where $\psi_{M,\Gamma(f_{\theta})}^{\delta}$ is from Def. 1, $\lambda_i, \mu_i \in \mathbb{R}$). Additional details of the algorithm can be found in Appendix E.

$$\begin{aligned} \text{Loss}(\theta, \lambda_1, \mu_2, \lambda_2, \mu_2) = & \mathbb{E}_{\substack{s \sim \mathcal{D} \\ s' \sim \Omega}} \left[L(\Gamma(f_{\theta})(s), x) + \left(\lambda_1 \psi_{M,\Gamma(f_{\theta})}^{\delta}(s) + \lambda_2 \psi_{M,\Gamma(f_{\theta})}^{\delta}(s') \right. \right. \\ & \left. \left. + \mu_1 \mathbb{1}_{(\lambda_1 > 0 \vee \psi > 0)} (\psi_{M,\Gamma(f_{\theta})}^{\delta}(s))^2 + \mu_2 \mathbb{1}_{(\lambda_2 > 0 \vee \psi > 0)} (\psi_{M,\Gamma(f_{\theta})}^{\delta}(s'))^2 \right) \right] \quad (2) \end{aligned}$$

4 EXPERIMENTS

Overview and baseline: We perform simulated experiments on three case studies, (a) CARLA (Dosovitskiy et al., 2017), (b) UVA/Padova Artificial Pancreas (Man et al., 2014), (c) Pybullet Drones (Panerati et al., 2021) (Figure 6). Our baseline is the augmented Lagrangian method which uses loss (2) but a standard parameterization $f_\theta(\cdot)$ rather than the constrained model (1). The augmented Lagrangian lacks guarantees with DNNs and non-convex constraints, and further, fails to conform on test data. Additional experiments, detailed descriptions and analysis can be found in Appendix F.

Case Study 1: CARLA – Conformance of a vehicle model to unicycle dynamics with emphasis on at-rest condition. We collect trajectories (3 states, 2 controls) from CARLA on a variety of terrains for dataset \mathcal{D} . With previous work Narasimhamurthy et al. (2019) having demonstrated the difficulty of learning a dynamics model that obeys Newton’s first law of motion with zero control, we uniformly sample at-rest data for the Ω dataset. Unicycle dynamics (M) encodes the at-rest condition. In Figure 7, we observe average constrained loss and max constrained loss on at-rest data (Ω) are lower by 4 and 3 orders of magnitude for our method in comparison to Vanilla and augmented Lagrangian. Further, our method is highly data-efficient, learning in less than 300 gradient steps.

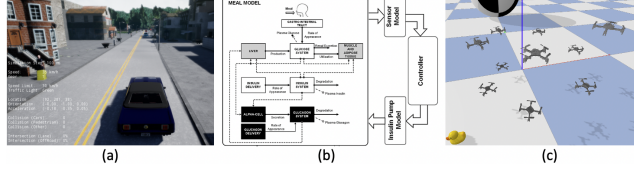


Figure 3: Depictions of high-fidelity simulators used: (a) CARLA (Dosovitskiy et al., 2017), (b) UVA/Padova Artificial Pancreas (Man et al., 2014), (c) Pybullet Drones (Panerati et al., 2021).

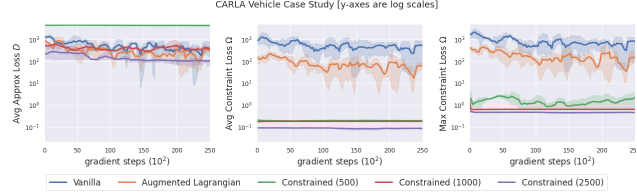


Figure 4: Plots of approximation loss on \mathcal{D} , average and maximum constraint loss on Ω (for 3 seeds) against steps for CARLA. Increasing memories reduces constraint loss.

Method	Max. violation	Avg. violation
Vanilla	3.8356	1.315
Aug. Lagrangian	3.8072	1.245
Constrained (1k)	0.9157	0.0092
Constrained (1.5k)	0.2047	0.0027
Constrained (2k)	0.1775	0.0026

Table 1: Delta-monotonicity analysis of “increasing insulin, decreases glucose” violation in AP models.

constrained models display negligible values (reducing further with more memories).

Case Study 3: PyBullet Drones – Conformance of drone models to quadrotor dynamics with emphasis on hover. We collect drone trajectories (20 states, 4 controls) with aerodynamics effects in Pybullet for \mathcal{D} . M is given by quadrotor dynamics. We create Ω with uniformly sampled inputs at hover. Like CARLA, we see (Figure 9) that approximation loss on \mathcal{D} is similar across methods but there is *upto a 6 order-of-magnitude decrease* in constraint losses on Ω with our method.

Case Study 2: Artificial Pancreas (AP) – Conformance of AP models to ARMAX model that encodes glucose-insulin constraints. We collect traces of glucose, insulin and meal quantities (30 states, 1 control) for patients with the AP simulator for \mathcal{D} . We uniformly sample the input space for Ω . For M , we train a constrained ARMAX model with negative weights for insulin, such that any increase in insulin inputs will reduce glucose predictions. Previously, Kushner et al. (2020) showed that this property (*a.k.a.* delta-monotonicity) was violated by neural networks. We report said violations in Table 2 where our

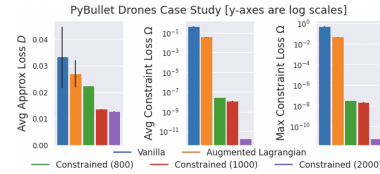


Figure 5: Bar charts of approx. loss on \mathcal{D} , avg. and max constraint loss on Ω (for 3 seeds) against steps after training completes for Drones.

5 CONCLUSION

We demonstrate how DNN training can be constrained using symbolic information which enforces adherence to natural laws. We report experiments on three case studies where our method achieves many fold reductions in constraint loss when compared to the augmented Lagrangian. In future work, we plan to create safety constrained policies.

REFERENCES

- Witold Brostow, Jean-Pierre Dussault, and Bennett L Fox. Construction of voronoi polyhedra. *Journal of Computational Physics*, 29(1):81–92, 1978. ISSN 0021-9991. doi: [https://doi.org/10.1016/0021-9991\(78\)90110-9](https://doi.org/10.1016/0021-9991(78)90110-9). URL <https://www.sciencedirect.com/science/article/pii/0021999178901109>. (Cited on 9)
- Sanjian Chen, James Weimer, Michael R Rickels, Amy Peleckis, and Insup Lee. Towards a model-based meal detector for type i diabetics. 2015. (Cited on 1)
- Miles Cranmer, Sam Greydanus, Stephan Hoyer, Peter Battaglia, David Spergel, and Shirley Ho. Lagrangian neural networks. *arXiv preprint arXiv:2003.04630*, 2020. (Cited on 2, 8)
- Alp Dener, Marco Andres Miller, Randy Michael Churchill, Todd Munson, and Choong-Seock Chang. Training neural networks under physical constraints using a stochastic augmented lagrangian approach. *arXiv preprint arXiv:2009.07330*, 2020. (Cited on 8)
- Franck Djeumou, Cyrus Neary, Eric Goubault, Sylvie Putot, and Ufuk Topcu. Neural networks with physics-informed architectures and constraints for dynamical systems modeling. In *Learning for Dynamics and Control Conference*, pp. 263–277. PMLR, 2022. (Cited on 1, 8)
- Alexey Dosovitskiy, German Ros, Felipe Codevilla, Antonio Lopez, and Vladlen Koltun. Carla: An open urban driving simulator. In *Conference on robot learning*, pp. 1–16. PMLR, 2017. (Cited on 4, 12)
- Thai Duong and Nikolay Atanasov. Hamiltonian-based neural ode networks on the se (3) manifold for dynamics learning and control. *arXiv preprint arXiv:2106.12782*, 2021. (Cited on 8)
- Marc Finzi, Ke Alexander Wang, and Andrew G Wilson. Simplifying hamiltonian and lagrangian neural networks via explicit constraints. *Advances in neural information processing systems*, 33: 13880–13889, 2020. (Cited on 1, 8)
- Ferdinando Fioretto, Pascal Van Hentenryck, Terrence WK Mak, Cuong Tran, Federico Baldo, and Michele Lombardi. Lagrangian duality for constrained deep learning. In *Joint European Conference on Machine Learning and Knowledge Discovery in Databases*, pp. 118–135. Springer, 2020. (Cited on 8)
- Bernd Fritzke. A growing neural gas network learns topologies. In *Proceedings of the 7th International Conference on Neural Information Processing Systems, NIPS’94*, pp. 625–632, Cambridge, MA, USA, 1994. MIT Press. (Cited on 3, 8, 11)
- Brian Goldfain, Paul Drews, Changxi You, Matthew Barulic, Orlin Velez, Panagiotis Tsiotras, and James M. Rehg. Autorally: An open platform for aggressive autonomous driving. *IEEE Control Systems Magazine*, 39(1):26–55, 2019. doi: 10.1109/MCS.2018.2876958. (Cited on 1)
- Eric Goubault and Sylvie Putot. Rino: Robust inner and outer approximated reachability of neural networks controlled systems. In *Computer Aided Verification: 34th International Conference, CAV 2022, Haifa, Israel, August 7–10, 2022, Proceedings, Part I*, pp. 511–523, Berlin, Heidelberg, 2022. Springer-Verlag. ISBN 978-3-031-13184-4. doi: 10.1007/978-3-031-13185-1_25. URL https://doi.org/10.1007/978-3-031-13185-1_25. (Cited on 9)
- Samuel Greydanus, Misko Dzamba, and Jason Yosinski. Hamiltonian neural networks. *Advances in neural information processing systems*, 32, 2019. (Cited on 8)
- Jayesh K Gupta, Kunal Menda, Zachary Manchester, and Mykel Kochenderfer. Structured mechanical models for robot learning and control. In *Learning for Dynamics and Control*, pp. 328–337. PMLR, 2020. (Cited on 8)
- Ramneet Kaur, Kaustubh Sridhar, Sangdon Park, Susmit Jha, Anirban Roy, Oleg Sokolsky, and Insup Lee. Codit: Conformal out-of-distribution detection in time-series data. *arXiv preprint arXiv:2207.11769*, 2022. (Cited on 12)
- Hoel Kervadec, Jose Dolz, Jing Yuan, Christian Desrosiers, Eric Granger, and Ismail Ben Ayed. Constrained deep networks: Lagrangian optimization via log-barrier extensions. In *2022 30th European Signal Processing Conference (EUSIPCO)*, pp. 962–966. IEEE, 2022. (Cited on 8)

- Taisa Kushner, Sriram Sankaranarayanan, and Marc Breton. Conformance verification for neural network models of glucose-insulin dynamics. In *Proceedings of the 23rd International Conference on Hybrid Systems: Computation and Control*, pp. 1–12, 2020. (Cited on 1, 4, 14)
- Lu Lu, Xuhui Meng, Zhiping Mao, and George Em Karniadakis. Deepxde: A deep learning library for solving differential equations. *SIAM Review*, 63(1):208–228, 2021a. (Cited on 8)
- Lu Lu, Raphael Pestourie, Wenjie Yao, Zhicheng Wang, Francesc Verdugo, and Steven G Johnson. Physics-informed neural networks with hard constraints for inverse design. *SIAM Journal on Scientific Computing*, 43(6):B1105–B1132, 2021b. (Cited on 3, 8, 11)
- Michael Lutter, Christian Ritter, and Jan Peters. Deep lagrangian networks: Using physics as model prior for deep learning. *arXiv preprint arXiv:1907.04490*, 2019. (Cited on 8)
- Robert Mahony, Vijay Kumar, and Peter Corke. Multirotor aerial vehicles: Modeling, estimation, and control of quadrotor. *IEEE Robotics and Automation magazine*, 19(3):20–32, 2012. (Cited on 1, 14)
- Chiara Dalla Man, Francesco Micheletto, Dayu Lv, Marc Breton, Boris Kovatchev, and Claudio Cobelli. The uva/padova type 1 diabetes simulator: new features. *Journal of diabetes science and technology*, 8(1):26–34, 2014. (Cited on 1, 4, 12, 13)
- Pablo Márquez-Neila, Mathieu Salzmann, and Pascal Fua. Imposing hard constraints on deep networks: Promises and limitations. *arXiv preprint arXiv:1706.02025*, 2017. (Cited on 1, 8)
- T.M. Martinetz, S.G. Berkovich, and K.J. Schulten. ‘neural-gas’ network for vector quantization and its application to time-series prediction. *IEEE Transactions on Neural Networks*, 4(4):558–569, 1993. doi: 10.1109/72.238311. (Cited on 3, 8, 11)
- Takashi Matsubara, Ai Ishikawa, and Takaharu Yaguchi. Deep energy-based modeling of discrete-time physics. *Advances in Neural Information Processing Systems*, 33:13100–13111, 2020. (Cited on 8)
- Regina Hunter Mladineo. Stochastic minimization of lipschitz functions. 1991. (Cited on 9)
- Thomas M. Moerland, Joost Broekens, and Catholijn M. Jonker. Model-based reinforcement learning: A survey. *CoRR*, abs/2006.16712, 2020. URL <https://arxiv.org/abs/2006.16712>. (Cited on 1)
- Yatin Nandwani, Abhishek Pathak, and Parag Singla. A primal dual formulation for deep learning with constraints. *Advances in Neural Information Processing Systems*, 32, 2019. (Cited on 8)
- Monal Narasimhamurthy, Taisa Kushner, Souradeep Dutta, and Sriram Sankaranarayanan. Verifying conformance of neural network models: Invited paper. In *2019 IEEE/ACM International Conference on Computer-Aided Design (ICCAD)*, pp. 1–8, 2019. doi: 10.1109/ICCAD45719.2019.8942151. (Cited on 1, 4, 8, 12)
- Jacopo Panerati, Hehui Zheng, SiQi Zhou, James Xu, Amanda Prorok, and Angela P. Schoellig. Learning to fly—a gym environment with pybullet physics for reinforcement learning of multi-agent quadcopter control. In *2021 IEEE/RSJ International Conference on Intelligent Robots and Systems (IROS)*, 2021. (Cited on 4, 12, 14)
- Y. Prudent and A. Ennaji. An incremental growing neural gas learns topologies. In *Proceedings. 2005 IEEE International Joint Conference on Neural Networks, 2005.*, volume 2, pp. 1211–1216 vol. 2, 2005. doi: 10.1109/IJCNN.2005.1556026. (Cited on 8)
- Maziar Raissi, Paris Perdikaris, and George E Karniadakis. Physics-informed neural networks: A deep learning framework for solving forward and inverse problems involving nonlinear partial differential equations. *Journal of Computational physics*, 378:686–707, 2019. (Cited on 8)
- Rajesh Rajamani. *Vehicle dynamics and control*. Springer Science & Business Media, 2011. (Cited on 1, 12)

- Sathya N Ravi, Tuan Dinh, Vishnu Suresh Lokhande, and Vikas Singh. Explicitly imposing constraints in deep networks via conditional gradients gives improved generalization and faster convergence. In *Proceedings of the AAAI Conference on Artificial Intelligence*, volume 33, pp. 4772–4779, 2019. (Cited on 1, 8)
- Manuel A Roehrl, Thomas A Runkler, Veronika Brandstetter, Michel Tokic, and Stefan Obermayer. Modeling system dynamics with physics-informed neural networks based on lagrangian mechanics. *IFAC-PapersOnLine*, 53(2):9195–9200, 2020. (Cited on 8)
- Guanya Shi, Xichen Shi, Michael O’Connell, Rose Yu, Kamyar Azizzadenesheli, Animashree Anandkumar, Yisong Yue, and Soon-Jo Chung. Neural lander: Stable drone landing control using learned dynamics. In *2019 International Conference on Robotics and Automation (ICRA)*, pp. 9784–9790. IEEE, 2019. (Cited on 1, 8)
- Kaustubh Sridhar and Srikant Sukumar. Finite-time, event-triggered tracking control of quadrotors. In *5th CEAS Specialist Conference on Guidance, Navigation & Control (EurGNC 19) Milano, Italy*, 2019. (Cited on 14)
- Kaustubh Sridhar, Radoslav Ivanov, Vuk Lesi, Marcio Juliato, Manoj Sastry, Lily Yang, James Weimer, Oleg Sokolsky, and Insup Lee. A framework for checkpointing and recovery of hierarchical cyber-physical systems. *arXiv preprint arXiv:2205.08650*, 2022. (Cited on 12)
- Yaofeng Desmond Zhong, Biswadip Dey, and Amit Chakraborty. Symplectic ode-net: Learning hamiltonian dynamics with control. *arXiv preprint arXiv:1909.12077*, 2019. (Cited on 8)

APPENDIX

A RELATED WORK

Enforcing constraints on neural networks: Imposing constraints on deep neural networks has been studied from various perspectives (Djeumou et al., 2022; Finzi et al., 2020; Márquez-Neila et al., 2017; Ravi et al., 2019; Lu et al., 2021b; Dener et al., 2020; Fioretto et al., 2020; Nandwani et al., 2019; Kervadec et al., 2022). These include constraints of symmetry and contact forces for dynamical systems in Djeumou et al. (2022), suitable constraints for specific Lagrangian or Hamiltonian neural networks in Finzi et al. (2020), human pose constraints in Márquez-Neila et al. (2017), path norm constraints on resnets in Ravi et al. (2019), partial differential equation (PDE) constraints for inverse design in Lu et al. (2021b), Focke-Planck constraints for fusion in Dener et al. (2020), fairness constraints in Fioretto et al. (2020), language label constraints in Nandwani et al. (2019), and segmentation constraints in Kervadec et al. (2022). All of these methods rely on the augmented Lagrangian method to train constrained neural networks. Solving the dual problem, *i.e.* converging to a stationary point for the min-max optimization is challenging with neural networks and non-convex constraints (Márquez-Neila et al., 2017). Further, the process is data-hungry and generalizes poorly in out-of-distribution data (Narasimhamurthy et al., 2019; Márquez-Neila et al., 2017; Ravi et al., 2019). Our focus in this work is to leverage the benefits of the augmented Lagrangian approach (its flexible loss function) but constrain the neural network by design, and with a guarantee, to remain within desirable output bounds computed using models that encode all desired constraints. In the process, we obtain several orders of magnitude reduction in constraint loss and learn with very few gradient steps.

Physics informed neural networks for dynamics models: Although our focus is on enforcing constraints, we also briefly discuss related ideas in physics-informed neural networks (Raissi et al., 2019; Márquez-Neila et al., 2017; Lu et al., 2021a; Lutter et al., 2019; Cranmer et al., 2020; Greydanus et al., 2019). Physics-informed architectures for dynamical systems in particular have been explored via specific Neural ODE structures for a class of systems (Duong & Atanasov, 2021; Zhong et al., 2019; Roehrl et al., 2020; Matsubara et al., 2020; Gupta et al., 2020; Shi et al., 2019) or via a broader Neural ODE structure for a class of vector fields (Djeumou et al., 2022), all towards learning continuous-time dynamics for robotics applications. Our constraining framework can be applied around any such Neural ODE. But moreover, our constraints can include black-box models and scale quickly to any state and action space unlike NeuralODEs which are restricted to systems with rigorous mathematical models (Raissi et al., 2019). Further, to present a general solution, we make no assumption on the architecture and to extend to applications beyond dynamics models in robotics (such as medicine, computing systems, and operations research), we learn discrete-time dynamics models in our experiments rather than continuous-time dynamics models.

B PRELIMINARIES ON NEURAL GAS AND VORONOI POLYHEDRONS

We define the idea of a *neural gas* (Fritzke, 1994; Prudent & Ennaji, 2005; Martinetz et al., 1993). From a given set of points embedded in a metric space, a growing neural gas algorithm has the ability to learn important topological relations in the form of a graph of prototypical points. It uses a simple Hebb-like learning rule to construct this graph.

Definition 3 (Neural Gas). *Neural Gas $\mathcal{G} := (\mathcal{A}, \mathcal{E})$, is composed of the following two components,*

1. *A set $\mathcal{A} \subset \mathcal{S}$ of the nodes of a network. Each node $m_i \in \mathcal{A}$ is called a memory in this paper.*
2. *A set $\mathcal{E} \subset \{(m_i, m_j) \in \mathcal{M}^2, i \neq j\}$ of edges among pairs of nodes, which inform about the topological structure of the data. The edges are unweighted.*

The edges in \mathcal{E} preserve the neighborhood relations among the data, and is useful in achieving a Voronoi-like partitioning of the data manifold. The graphical structure of a neural gas makes it much more appealing to algorithmically resolve neighborhood relations. For a given node m_i , let us denote \mathcal{E}^i as the set of neighbors of m_i according to \mathcal{G} . For most practical purposes in a control setting, the spaces \mathcal{S} and \mathcal{X} are embedded in Euclidean spaces \mathbb{R}^t , and \mathbb{R}^d respectively, where $t \geq d$. Where, $t - d$ is the dimension of control input. Let k be the cardinality of $\mathcal{A} : \{m_1, m_2, m_3, \dots, m_k\}$. Then,

we can define the Voronoi polyhedron (Brostow et al., 1978), around a given point m_i in the following fashion.

Definition 4 (Voronoi Polyhedron). *For a point m_i , the Voronoi polyhedron $\mathcal{S}_v^i \in \mathcal{S}$ can be defined using the Euclidean distance function $d : \mathcal{S} \times \mathcal{S} \mapsto \mathbb{R}$ as,*

$$\mathcal{S}_v^i = \{s \in \mathcal{S} \mid d(s, m_i) < d(s, m_j) \quad \forall j \in \mathcal{E}^i\}$$

In practice, constructing the Voronoi polyhedron \mathcal{S}_v^i can be achieved in the following way. Given points which are neighbors m_i and m_j , it is possible to compute a line segment l_{ij} which connects them. Let us denote the perpendicular bisector of l_{ij} as the linear inequality $H_{ij}(s) > 0$. For any point s which is in the same side of H_{ij} as m_i the inequality holds. The reverse is true for the half space constraint H_{ji} . This gives us an algorithm to compute $\mathcal{S}_v^i = \bigcap_{j \in \mathcal{E}^i} H_{ij}$. Thus, given a

set of k nodes the Voronoi tessellation induces a splitting of the space \mathcal{S} into a set of disjoint sets $\mathcal{S}^1, \mathcal{S}^2, \dots, \mathcal{S}^k$. We drop the subscript v for the rest of the paper. Our guarantees of constraint satisfaction is over the union of these subsets.

C APPROXIMATING MODEL CONSTRAINTS

Assume a (relatively small) subset $\mathcal{S}_a \subset \mathcal{S}$, and $M^j(s)$ denote the j -th output of the model at input s . We wish to compute the interval $I_a^j := [\min_{s \in \mathcal{S}_a} M^j(s), \max_{s \in \mathcal{S}_a} M^j(s)]$. Assume that $\forall s \in \mathcal{S}_a, f_\theta^j(s) \in I'$, and $I' \subseteq I_a^j$. Where I' is the interval bound on values of f_θ^j in \mathcal{S}_a . Then $\max_{s \in \mathcal{S}_a} |M^j(s) - f_\theta^j(s)| \leq |I_a^j|$.

Now, in practice it is hard to precisely compute the interval I_a^j for black-box models M . Meaning that we would resort to estimating the min and max of M^j using sampling based techniques. There exists a stochastic optimization algorithm to estimate the true maxima of a Lipschitz function on a bounded domain (Mladineo, 1991). Here we follow a simple sampling based rendition to estimate I_a^j . We denote $[k]$ as the list of numbers from $0 \dots k-1$. Next, we note the following lemma.

Lemma 1. *Let $g : \mathbb{R}^t \rightarrow \mathbb{R}$ be an L_g -Lipschitz continuous function on a closed and compact set \mathcal{S}_a , and l and u be its estimated lower and upper bounds. Then, $\forall z \in [l, u], \max_{s \in \mathcal{S}_a} |g(s) - z| < L_g |\mathcal{S}_a|$.*

Proof : The proof can be found in the Appendix.

With $\mathcal{S}_a \subset \mathbb{R}^t$, let l and u be the estimated minima and maxima of M^j . Thus, if $\forall s \in \mathcal{S}_a, f_\theta^j(s) \in [l, u]$, then $\max_{s \in \mathcal{S}_a} |M^j(s) - f_\theta^j(s)| \leq L_{M^j} |\mathcal{S}_a|$. Now, across all dimensions $j \in [d]$, let $L_M = \max_j L_{M^j}$ then, $\|f_\theta(s) - M(s)\|_\infty < L_M |\mathcal{S}_a|$. Assume a^* , to be the largest partition induced by the neural gas \mathcal{G} , then setting $\delta = L_M |\mathcal{S}_{a^*}|$ ensures satisfaction of model constraint $\psi_{M, f_\theta}^\delta$ in Definition 1. This bound can be made much tighter in practice if the model M is known in an analytical form. Allowing tight computations of its limits possible using techniques like interval arithmetic and Taylor models (Goubault & Putot, 2022)

So, given a set \mathcal{S} and using neural gas \mathcal{G} , we have a partitioning of $\mathcal{S} = \bigcup_{i \in [k]} \mathcal{S}^i$. Let us denote this

set of partitions of \mathcal{S} as $\mathcal{P}_\mathcal{S} := \{\mathcal{S}^1, \mathcal{S}^2, \dots, \mathcal{S}^k\}$. Also, for each subset \mathcal{S}^i we can compute range estimate $I_i \subset \mathcal{X}$, which respects the constraint $\psi_{M, f_\theta}^\delta$. In the following discussions, let us refer to this constraint map as $\mathcal{C}_{M, \delta} : \mathcal{P}_\mathcal{S} \mapsto \mathcal{I}^d$. Where, \mathcal{I}^d is a d -dimensional interval in \mathbb{R}^d . For a subset in $\mathcal{P}_\mathcal{S}$, $\mathcal{C}_{M, \delta}$ returns the appropriate output range.

D PROOF OF THEOREM 1

Theorem (Approximation Error). *Assume real and continuous functions $f, f_\theta : \mathcal{S} \rightarrow \mathcal{X}, \forall s \in \mathcal{S}$, if $\|f_\theta(s) - f(s)\|_\infty < \epsilon$, then $\|\Gamma_{\mathcal{P}_\mathcal{S}}(f_\theta)(s) - f(s)\|_\infty < 2\epsilon + \alpha \max_{\mathcal{S}^k \in \mathcal{P}_\mathcal{S}} |\mathcal{S}^k|$, where α is some constant.*

Proof : Assume a generic input $s \in \mathcal{S}$, and $s \in \mathcal{S}^q$ for some $q \in [\mathcal{P}_\mathcal{S}]$. Additionally, let I^q be the interval constraint imposed by $\Gamma_{\mathcal{P}_\mathcal{S}}$ on f_θ using the map $\mathcal{C}_{M, \delta}$. Since the sets \mathcal{S} and \mathcal{X} are embedded

in the real spaces \mathbb{R}^t and \mathbb{R}^d respectively, we can analyze the error incurred along each dimension. Also, we drop the subscript and denote the constraining operator as simply Γ since the partition remains fixed for the remainder of the results.

x_j refers to the j^{th} element of x . Let us pick a dimension $w \in [t]$, we define the lower correction set $\gamma_{w,l} : \{s \mid \Gamma(f_\theta)(s)_w \geq f_\theta(s)_w \text{ and } s \in \mathcal{S}^q\}$. Intuitively, this is the set of points in \mathcal{S}^q , which need a correction due to underflow. Let us denote the difference function as $\Delta_{w,l}$,

$$\Delta_{w,l}(s) := \begin{cases} \Gamma(f_\theta)(s)_w - f_\theta(s)_w & \text{when } s \in \gamma_{w,l} \cap \mathcal{S}^q \\ 0 & \text{when } s \in \mathcal{S}^q \setminus \gamma_{w,l} \end{cases} \quad (3)$$

We can similarly define the upper correction set $\gamma_{w,u} \subseteq \mathcal{S}^q$ and the difference function as $\Delta_{w,u}(s) = f_\theta(s)_w - \Gamma(f_\theta)(s)_w$ for $s \in \gamma_{w,u} \cap \mathcal{S}^q$ and 0 for anywhere in $\mathcal{S}^q \setminus \gamma_{w,u}$.

Now the following is true, for $s \in \gamma_{w,l} : 0 \leq \Delta_{w,l}(s) \leq I_{w,l}^q - \min_{s \in \mathcal{S}^q} f_\theta(s)_w$. This is simply due to the bound respected by $\Gamma(f_\theta)(s)_w$. Due to very similar reasons the following is true as well : $0 \leq \Delta_{w,u}(s) \leq \max_{s \in \mathcal{S}^q} f_\theta(s)_w - I_{w,u}^q$. Next, we wish to bound the following quantity:

$|\Gamma(f_\theta)(s)_w - f(s)_w|$. The difference between the constrained function and ground truth. Then,

$$\begin{aligned} \Gamma(f_\theta)(s)_w - f(s)_w &= f_\theta(s)_w + \Delta_{w,l}(s) - \Delta_{w,u}(s) - f(s)_w \\ &= (f_\theta(s)_w - f(s)_w) + (\Delta_{w,l}(s) - \Delta_{w,u}(s)) \end{aligned}$$

The first equality is simply because \mathcal{S}_q can be expressed as a union of the following disjoint sets $\{\gamma_{w,l} \cap \mathcal{S}_q, \gamma_{w,u} \cap \mathcal{S}_q, \mathcal{S}^q \setminus (\gamma_{w,l} \cup \gamma_{w,u})\}$. Therefore, we can write the following,

$$\begin{aligned} \Gamma(f_\theta)(s)_w - f(s)_w &\leq \epsilon + (I_{w,l}^q - \min_{s \in \mathcal{S}^q} f_\theta(s)_w) \\ \Gamma(f_\theta)(s)_w - f(s)_w &\geq -\epsilon - (\max_{s \in \mathcal{S}^q} f_\theta(s)_w - I_{w,u}^q) \end{aligned}$$

Note, the R.H.S of the above equation is negative. Then using the bound on the upper limit of absolute values, we get the following,

$$\begin{aligned} |\Gamma(f_\theta)(s)_w - f(s)_w| &\leq \epsilon + \underbrace{(I_{w,l}^q - \min_{s \in \mathcal{S}^q} f_\theta(s)_w)}_{\geq 0} + \epsilon + \underbrace{(\max_{s \in \mathcal{S}^q} f_\theta(s)_w - I_{w,u}^q)}_{\geq 0} \\ &= 2\epsilon + \left(\max_{s \in \mathcal{S}^q} f_\theta(s)_w - \min_{s \in \mathcal{S}^q} f_\theta(s)_w \right) - \underbrace{(I_{w,u}^q - I_{w,l}^q)}_{\text{constraining width}} \end{aligned} \quad (4)$$

Thus, we can bound $\|\Gamma(f_\theta)(s) - f(s)\|_\infty$ in the following fashion, for $s \in \mathcal{S}^q$:

$$\begin{aligned} \|\Gamma(f_\theta)(s) - f(s)\|_\infty &\leq 2\epsilon + \max_{w \in [d]} \left(\left(\max_{s \in \mathcal{S}^q} f_\theta(s)_w - \min_{s \in \mathcal{S}^q} f_\theta(s)_w \right) - \underbrace{(I_{w,u}^q - I_{w,l}^q)}_{=|I^q|_w \geq 0} \right) \\ &\leq 2\epsilon + \max_{w \in [d]} (L_{\theta,w} |\mathcal{S}^q|) = 2\epsilon + |\mathcal{S}^q| \max_{w \in [d]} (L_{\theta,w}) \end{aligned}$$

Now, setting $\alpha = L_\theta$, where L_θ is the global Lipschitz constant of f_θ , we can write,

$$\|\Gamma(f_\theta)(s) - f(s)\|_\infty \leq 2\epsilon + \alpha \max_{\mathcal{S}^q \in \mathcal{P}_S} |\mathcal{S}^q|, \forall s \in \mathcal{S} \quad \square$$

We draw the attention of the reader to the terms in inequality 4: $(I_{w,l}^q - \min_{s \in \mathcal{S}^q} f_\theta(s)_w)$ and $(\max_{s \in \mathcal{S}^q} f_\theta(s)_w - I_{w,u}^q)$. Similar to Lemma in Appendix C it can be shown that this difference goes down with the size of the set \mathcal{S}^q . In other words having finer Voronoi partitions gives lower approximation error.

Algorithm 2 Training a Constrained Neural Network Dynamics Model**Input:** Dataset $\mathcal{D} = \{(s, x)_i\}_{i \in [N_{\mathcal{D}}]}$, Knowledge M , DNN architecture $f_{\theta}(\cdot)$ **Output:** Constrained neural network dynamics model $\Gamma(f_{\theta})(\cdot)$ **Parameters:** Number of memories n_{memories} , batch sizes $N_{\mathcal{D}_{\text{batch}}}, N_{\Omega_{\text{batch}}}$, $0 \leq \gamma < 1$, N_Steps, update_freq

```

1: Generate input samples  $\Omega = \{(s')_i\}_{i \in [N_{\Omega}]}$  // unlabelled dataset
2:  $D|_{\text{inputs}} = \{(s)_i\}_{i \in [N_{\mathcal{D}}]} \cup \{(s')_i\}_{i \in [N_{\Omega}]}$  // combine inputs in both datasets
3: Memories  $\mathcal{A}$ , edges  $\mathcal{E} \leftarrow \text{NeuralGas}(D|_{\text{inputs}}, n_{\text{memories}})$  // topology of input space
4:  $\mathcal{S}^1, \dots, \mathcal{S}^j, \dots \leftarrow \text{VoronoiCells}(\mathcal{A}, \mathcal{E})$  // partitions in input space
5: for each voronoi cell  $\mathcal{S}^j$  do
6:   Sample points inside the cell, propagate through model  $M$ , and compute lower and upper bounds
    $I_{\text{low}}^j = \min_{s \sim \mathcal{S}^j} M(s)$  and  $I_{\text{up}}^j = \max_{s \sim \mathcal{S}^j} M(s)$ 
7: end for
8: for  $s$  in  $D, \Omega$  do
9:    $\mathcal{S}_j \leftarrow \text{FindVoronoiCell}(s, \mathcal{A})$ 
10:  Set  $\text{Lo}(s), \text{Up}(s) \leftarrow I_{\text{low}}^j, I_{\text{up}}^j$  // output bounds for datasets
11: end for
12: for step in N_Steps do
13:  Sample batches  $\mathcal{D}_{\text{batch}} = \text{Sample}(D, N_{\mathcal{D}_{\text{batch}}})$ ,  $\Omega_{\text{batch}} = \text{Sample}(\Omega, N_{\Omega_{\text{batch}}})$ 
14:  Set  $\text{Lo}(s, \text{step}) = \text{Lo}(s) - \gamma^{\text{step}} (\text{Up}(s) - \text{Lo}(s))$  and  $\text{Up}(s, \text{step}) = \text{Lo}(s) + \gamma^{\text{step}} (\text{Up}(s) - \text{Lo}(s))$ 
15:  Compute  $\Gamma(f_{\theta})(\cdot)$  for  $\mathcal{D}_{\text{batch}}$  and  $\Omega_{\text{batch}}$  using  $\text{Lo}(s, \text{step})$  and  $\text{Up}(s, \text{step})$  // constrained DNN (5)
16:  Compute  $\text{Loss}(\theta, \lambda, \mu)$  // augmented Lagrangian loss (6) or vanilla approximation loss
17:   $\theta \leftarrow \text{Optimization\_Step}(\text{Loss}, \theta, \mathcal{D}_{\text{batch}}, \Omega_{\text{batch}})$ 
18:  if step % update_freq == 0 then
19:     $\lambda_1, \lambda_2, \mu_1, \mu_2 \leftarrow \text{Update\_Step}(\psi_{M, \Gamma(f_{\theta})}^{\delta}, \lambda, \mu)$ 
20:  end if
21: end for
22: return  $\Gamma(f_{\theta})(\cdot)$ 

```

E DETAILED ALGORITHM FOR TRAINING A CONSTRAINED NEURAL NETWORK DYNAMICS MODEL

We detail our Algorithm in this section. The inputs to the algorithm are a state transitions dataset D containing ((state, control), (next state)) pairs (s, x) , model M , and architecture $f_{\theta} : \mathcal{S} \rightarrow \mathcal{X}$.

Algorithm 2 First (line 1), we generate the unlabelled Ω dataset which consists of only inputs to the model $s' \in \mathcal{S}$ by sampling throughout the input space but with particular emphasis on relevant regions in \mathcal{S} . Then, (lines 2 – 4), we use the unsupervised neural gas algorithm (Martinetz et al., 1993; Fritzke, 1994) to obtain the neural gas graph $\mathcal{G} = (\mathcal{A}, \mathcal{E})$. We utilize these memories and edges, to create partitions of the input space as voronoi cells with memories at their center. In each voronoi cell, we sample points, propagate them through the model M and obtain the upper and lower limits along each dimension of the output space \mathcal{X} (lines 5-7). This creates the constraint map C . Using this, we can find the lower and upper bounds of each point in \mathcal{D} and Ω (lines 8-12). First, we locate the corresponding voronoi cell, and then use the bounds computed in Line 6. Finally, we can train the constrained neural network (denoted $\Gamma(f_{\theta})(\cdot)$) as follows,

$$\Gamma(f_{\theta})(s) = \text{Lo}(s) + \sigma(f_{\theta}(s)) (\text{Up}(s) - \text{Lo}(s)) \quad (5)$$

where $f_{\theta} : \mathcal{S} \rightarrow \mathcal{X}$ is a parameterized function which maps from the input space to output space, and $\sigma(x) : \mathcal{X} \rightarrow [0, 1]$ is the sigmoid function. Equation 5 is but one realization of the constraining operator discussed in Definition 2. Our loss function is the augmented Lagrangian loss (Lu et al., 2021b) itself and is given below (where $\psi_{M, \Gamma(f_{\theta})}^{\delta}(s) = \delta - \|M(s) - \Gamma(f_{\theta})(s)\|$).

$$\begin{aligned} \text{Loss}(\theta, \lambda_1, \mu_2, \lambda_2, \mu_2) = & \mathbb{E}_{\substack{s' \sim \mathcal{D} \\ s' \sim \Omega}} \left[L(\Gamma(f_{\theta})(s), x) + \left(\lambda_1 \psi_{M, \Gamma(f_{\theta})}^{\delta}(s) + \lambda_2 \psi_{M, \Gamma(f_{\theta})}^{\delta}(s') \right) \right. \\ & \left. + \mu_1 \mathbb{1}_{(\lambda_1 > 0 \vee \psi > 0)} (\psi_{M, \Gamma(f_{\theta})}^{\delta}(s))^2 + \mu_2 \mathbb{1}_{(\lambda_2 > 0 \vee \psi > 0)} (\psi_{M, \Gamma(f_{\theta})}^{\delta}(s'))^2 \right] \quad (6) \end{aligned}$$

We can then train the neural network by back-propagating through the constrained neural network (lines 12-16). We enhance gradient feedback under constrained outputs with an exponential schedule

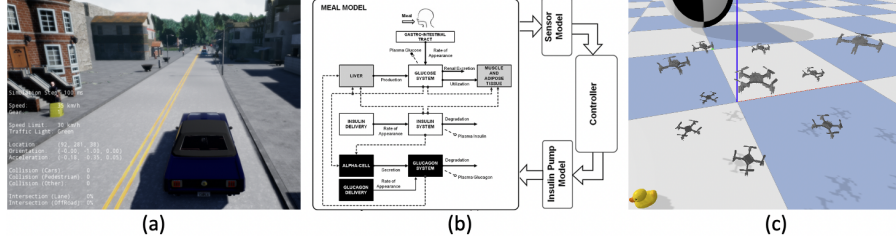


Figure 6: Depictions of high-fidelity simulators used in experiments: (a) CARLA (Dosovitskiy et al., 2017), (b) UVA/Padova Artificial Pancreas (Man et al., 2014), (c) Pybullet Drones (Panerati et al., 2021).

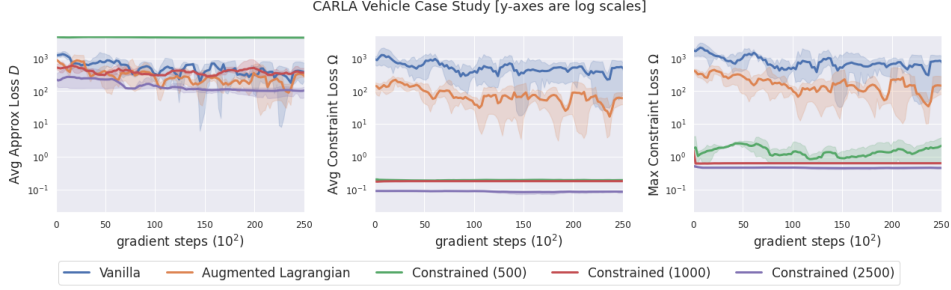


Figure 7: Plots of approximation loss on \mathcal{D} , average constraint loss on Ω , and maximum constraint loss on Ω (for 3 random seeds) against steps for the CARLA Vehicle case study.

on the lower and upper bounds (line 13). We also intermittently update the slack variables through a schedule or as a gradient ascent step on the value of the constraint $\psi_{M,\Gamma(f_\theta)}^\delta$ (lines 17-19).

F COMPLETE EXPERIMENTAL EVALUATION

Overview and baseline: We perform simulated experiments on three case studies. We create a dataset \mathcal{D} from high-fidelity simulators that can closely represent reality in each case study. These are depicted in Figure 6. Our baseline is the augmented Lagrangian method which utilizes the loss function in (2) but uses a standard parameterization $f_\theta(\cdot)$ rather than the constrained model given in (1). The augmented Lagrangian method lacks guarantees on constraint satisfaction with deep neural networks and non-convex constraints. We observe that augmented Lagrangian in fact fails to achieve conformance on in-distribution transitions in the test set.

Case Study 1: CARLA – Conformance of a vehicle model to unicycle dynamics with emphasis on at-rest condition. In the first case study, we collect trajectories of x position, y position, heading, velocity, yaw rate from the CARLA simulator (Dosovitskiy et al., 2017; Kaur et al., 2022) on a variety of terrains and environments (See Figure 6(a)) for our \mathcal{D} dataset. With previous work Narasimhamurthy et al. (2019) having demonstrated the difficulty of learning a dynamics model that predicts no change in state when a vehicle is at rest, we uniformly sample at-rest data for the augmenting dataset Ω . Unicycle dynamics (Rajamani, 2011; Sridhar et al., 2022) are chosen as the model M . This implicitly encodes the at-rest condition. We have 15,000 training points, 2000 test points in each of \mathcal{D} and Ω . We select 500, 1000 and 2500 memories to observe the performance with increasing partitions in the training distribution. We use a two-layer MLP with 1024 neurons and set γ to zero in each layer in this case study. We utilize the Adam optimizer in all case studies and choose a learning rate by grid searching in $[0.001, 0.1]$. Lastly, we set the training batch size to 64 for both \mathcal{D} and Ω datasets.

We observe, in Figure 7, that the approximation loss for constrained methods is either similar to or slightly higher than the Vanilla and augmented Lagrangian. This is expected in light of Theorem 1. The average constrained loss and max constrained loss on the augmenting dataset Ω are significantly improved, *by 4 and 3 orders of magnitude respectively* for our method in comparison to Vanilla and

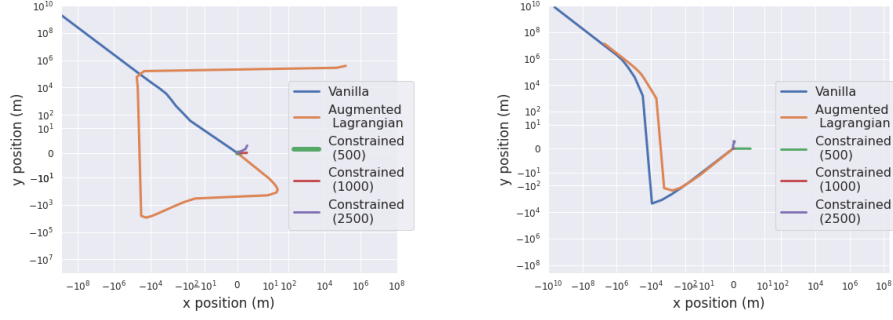


Figure 8: Analysis of CARLA model prediction drift starting from origin at rest when given zero control inputs for 20 timesteps for random seed of 0 [LEFT] and random seed of 1 [RIGHT].

augmented Lagrangian. Moreover, with increasing memories, the constraint loss, both average and maximum on Ω , improve consistently. We also notice that constrained training is highly data-efficient, learning in less than 300 gradient steps unlike the 12000 required by the Augmented Lagrangian. In Figure 8, we analyze each of the models’ predictions starting from the origin at rest, and given zero control inputs for 20 timesteps. We clearly observe that both Vanilla and augmented Lagrangian models predict large drift to the top-left Constrained models, on the other hand, accurately predict little to no movement.

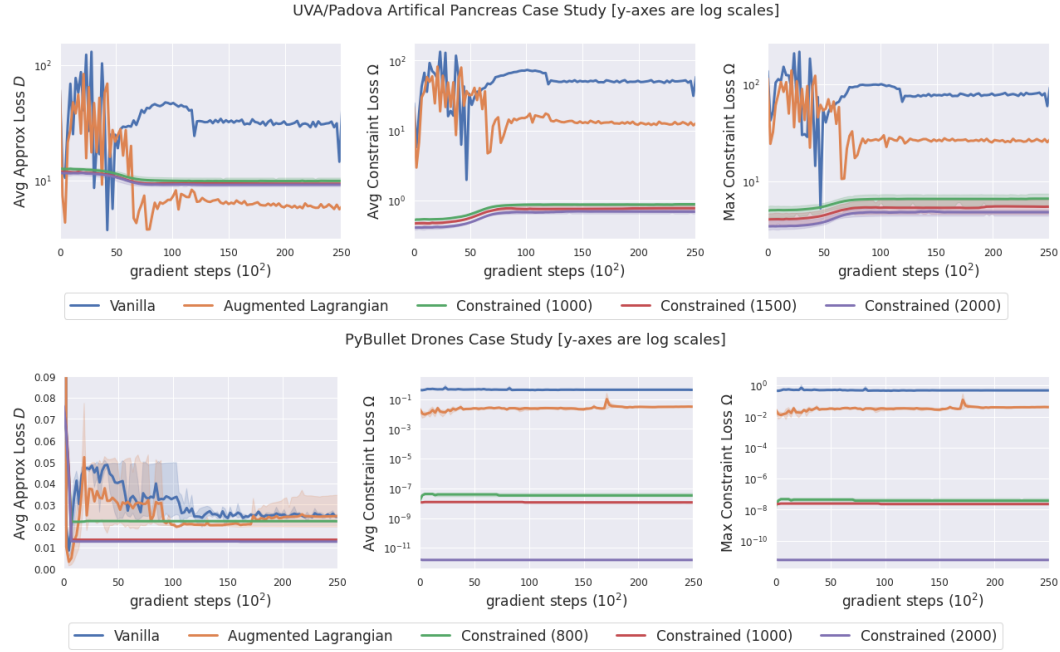


Figure 9: Plots of approximation loss on \mathcal{D} , average constraint loss on Ω , and maximum constraint loss on Ω (for 3 random seeds) against gradient steps for Artificial Pancreas (*top row*), and PyBullet Drones (*second row*) case studies.

Case Study 2: Artificial Pancreas (AP) – Conformance of AP models to ARMAX model that encodes glucose-insulin constraints. We collect traces of glucose, insulin and meal quantities for a patient with the UVA/Padova simulator (See Figure 6(c)) (Man et al., 2014) to create the \mathcal{D} dataset. The states consist of a 30 elements— 10 historical values of glucose, insulin and meals respectively. The model is expected to predict the glucose 5 steps in the future. Each timestep spans 5 minutes. The initial value of glucose and carbohydrates are randomly chosen in $[150, 190]$, $[50, 150]$ respectively. We also uniformly sample the state space with emphasis on low glucose initial values in $[120, 150]$

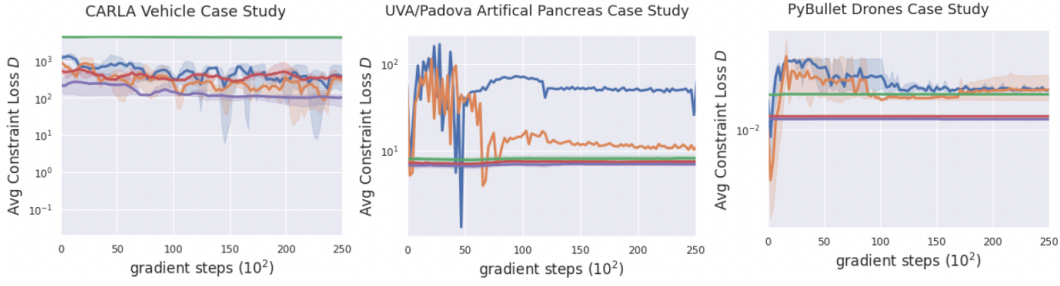


Figure 10: Average constraint loss on \mathcal{D} in CARLA, Artificial Pancreas, and PyBullet Drones case studies.

and low carbohydrates to create the Ω dataset. We have 18,750 training points, 2500 test points in each of \mathcal{D} and Ω . Moreover, for our model M , we train a constrained ARMAX model such that any increase in insulin, will reduce glucose. This is accomplished by constraining insulin weights to be negative in the ARMAX model. In Figure 9, we observe that approximation loss on \mathcal{D} is similar across all methods with a slight advantage in the favour of our constrained training. Yet, constrained neural networks outperform vanilla and Lagrangian by an order of magnitude in conforming to the ARMAX model on the Ω and \mathcal{D} datasets. We use a three-layer neural network architecture with 20 neurons in each layer and set $\gamma = 0.99$ in this case study.

The delta-monotonicity property of such models in (Kushner et al., 2020), refers to the following - everything else remaining fixed, increasing insulin should lead to reduction in blood glucose prediction. In order to test this property we increase the insulin value in each input trace of test set by a random amount in $[0.6, 1.0]$ and observe the prediction. We report this in Table 2. We observe that vanilla and Lagrangian models violate the constraint by a large margin, whereas constrained models increase the prediction by nearly zero amount.

Method	Max. violation	Avg. violation
Vanilla	3.8356	1.315
Aug. Lagrangian	3.8072	1.245
Constrained (1k)	0.9157	0.0092
Constrained (1.5k)	0.2047	0.0027
Constrained (2k)	0.1775	0.0026

Table 2: Delta-monotonicity analysis of “increasing insulin, decreases glucose” violation in AP models on subsets of test data.

Case Study 3: PyBullet Drones – Conformance of

drone models to quadrotor dynamics with emphasis on hover. We collect circular flight trajectories of 6 drones (See Figure 6(b)) with aerodynamics effects (drag, downwash, ground effect) included in the Pybullet Drones environment (Panerati et al., 2021) to create the \mathcal{D} dataset. The states consist of 20 items – x, y, z positions and velocities; roll, pitch, yaw and their rates; quaternions, and rpms of each of the four motors. The controls consist of 4 rpm commands. Our model M is given by the quadrotor dynamics (Mahony et al., 2012; Sridhar & Sukumar, 2019). For emphasis on hover, we uniformly sample states across the state distribution and uniformly sample controls for balancing gravity (and hence hovering in-place) to create the Ω dataset. We have 15,000 training points, 2000 test points in each of \mathcal{D} and Ω . We vary the number of memories from 800, 1000, to 2000. We use a two-layer MLP with 1024 neurons in each layer and set γ to zero in this case study.

Similar to CARLA, we see (in Figure 9) that approximation loss on \mathcal{D} is similar across all methods but there is *upto a 6 order-of-magnitude decrease* in the average and maximum constraint loss on Ω with our constrained training algorithm. We also observe a rather large increase in performance from 1000 to 2000 memories. We also plot the average constraint loss on \mathcal{D} for all case studies in Figure 10.